nature COMMUNICATIONS

OPEN

ARTICLE

Received 10 May 2011 | Accepted 14 Sep 2011 | Published 11 Oct 2011

DOI: 10.1038/ncomms1510

Travelling and splitting of a wave of *hedgehog* expression involved in spider-head segmentation

Masaki Kanayama[1,2], Yasuko Akiyama-Oda[1], Osamu Nishimura[3,4], Hiroshi Tarui[3,†], Kiyokazu Agata[4] & Hiroki Oda[1,2]

During development segmentation is a process that generates a spatial periodic pattern. Peak splitting of waves of gene expression is a mathematically predicted, simple strategy accounting for this type of process, but it has not been well characterized biologically. Here we show temporally repeated splitting of gene expression into stripes that is associated with head axis growth in the spider *Achaearanea* embryo. Preceding segmentation, a wave of *hedgehog* homologue gene expression is observed to travel posteriorly during development stage 6. This stripe, co-expressing an *orthodenticle* homologue, undergoes two cycles of splitting and shifting accompanied by convergent extension, serving as a generative zone for the head segments. The two *orthodenticle* and *odd-paired* homologues are identified as targets of Hedgehog signalling, and evidence suggests that their activities mediate feedback to maintain the head generative zone and to promote stripe splitting in this zone. We propose that the 'stripe-splitting' strategy employs genetic components shared with *Drosophila* blastoderm subdivision, which are required for participation in an autoregulatory signalling network.

[1] JT Biohistory Research Hall, 1-1 Murasaki-cho, Takatsuki, Osaka 569-1125, Japan. [2] Department of Biological Sciences, Graduate School of Science, Osaka University, Osaka, Japan. [3] Genome Resource and Analysis Unit, Center for Developmental Biology, RIKEN, 2-2-3 Minatojima-minamimachi, Chuo-ku, Kobe, Hyogo 650-0047, Japan. [4] Department of Biophysics & Global COE, Graduate School of Science, Kyoto University, Kitashirakawa-Oiwake, Sakyo-ku, Kyoto 606-8502, Japan. †Present address: Omics Science Center, Yokohama Institute, RIKEN, 1-7-22 Suehiro-cho, Tsurumi-ku, Yokohama 230-0045, Japan. Correspondence and requests for materials should be addressed to H.O. (email: hoda@brh.co.jp).

Animal segmentation, which generates a spatial, periodic pattern, has been studied using various organisms[1–3] and serves as a simple platform to study the mathematical basis of biological pattern formation[4–7]. 'Subdivision' and 'oscillation' are two major categories of animal segmentation strategies (Fig. 1a,b). The former is represented by segmentation of the blastoderm of the long-germ insect *Drosophila*, which requires a relatively complex readout of morphogen gradients pre-established in a relatively large field and a hierarchy of gene interactions[8,9]. The latter is represented by segmentation of the vertebrate paraxial mesoderm, which requires a time-delayed autorepression system that achieves rhythmic oscillation to generate new, solitary, travelling waves successively[1,10–13]. A similar oscillatory mechanism might be involved in the segmentation that occurs sequentially in the posterior growth zone in embryos of short-germ arthropods, such as spiders[14].

Although mathematical modelling of *Drosophila* and vertebrate segmentation has been attempted based on experimental observations[15–18], further theoretical approaches, particularly numerical analyses of chemical reactions and diffusion, have led to the proposal of different pattern-forming systems that might potentially be applied to animal segmentation. Two-component autocatalytic reaction–diffusion systems may cause successive insertion of new activator peaks between pre-existing activator peaks[19–21] (Fig. 1c) and repeated cycles of splitting and shifting of pre-existing activator peaks[6,19,22] (Fig. 1d). Both the insertion and the splitting of activator peaks are promoted by field growth. Although stained embryos, which indicate that a domain of gene expression is resolved into multiple stripes or patches in a relatively short time, have been described[23,24], 'splitting' events in the context of animal segmentation have not been well characterized in cellular and molecular terms.

The present work is focused on head segmentation in embryos of the spider *Achaearanea tepidariorum*. In these embryos, cellularization is complete at or before the 16-nucleus stage[25], indicating that all of their segmentation processes occur in a cellular environment. The segmented germ band of the embryos is divided into three regions corresponding to the head (cephalon), thorax and opisthosoma. The head bears two pairs of appendages, the chelicerae (Ch) and the pedipalps (Pp), and the thorax has four pairs of appendages, which are the walking legs (L1-4). The *A. tepidariorum* gene *At-hedgehog* (*At-hh*)[26], a homologue of the *Drosophila* segment polarity *hh* gene encoding a secreted signalling protein, is expressed on the future anterior side of the embryo[27]. The *At-hh* expression begins from approximately early stage 3 (ref. 27), and later, *At-hh* serves as an early molecular indicator for head and opisthosomal segmentation[23,26,27]. Absence of *At-hh* activity results in severe caudalization[27]. The initial expression of the *A. tepidariorum* homologue of the *Drosophila* head gap-like *orthodenticle* (*otd*) gene, *At-otd*[28], requires strong Hh signalling inputs[27]. This *At-otd* expression is essential for the specification of the entire head region[23]. However, little is known about stripe-forming processes related to spider-head segmentation.

In this study, taking advantage of the spider model, we identify 'stripe-splitting' segmentation, which is associated with the convergent extension that elongates the spider-head axis. Based on observations at the cellular and molecular levels, we define a new category of segmentation strategy, split-type segmentation. Functional analyses lead us to propose that split-type spider-head segmentation requires an autoregulatory signalling network in which *At-hh*, *At-otd*, and other homologues of *Drosophila* segmentation genes participate.

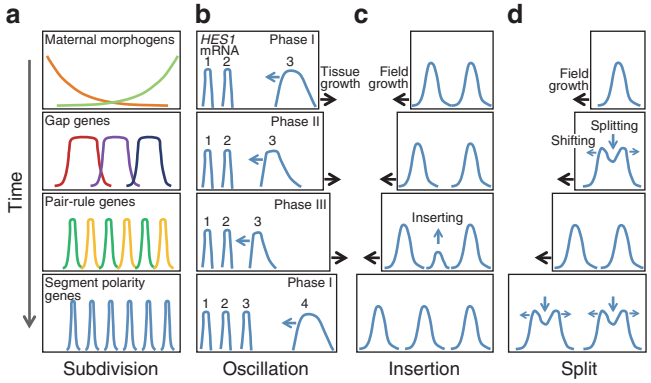

Figure 1 | Various strategies to generate a spatial periodic pattern. Blue curved lines indicate profiles of authentic or hypothetical segmental gene expression along the axis of the field. Differences are observed in how the new waves originate. (**a**) 'Subdivision' in segmentation of the *Drosophila* blastoderm embryo. Hierarchical cascades of maternal morphogens (shown in orange and light green), gap genes (shown in red, purple and dark blue), and pair-rule genes (shown in green and yellow) subdivide the embryo into progressively smaller domains and eventually lead to initiation of the expression of segment polarity genes nearly simultaneously in all of the forming segments[8,9]. For simplicity, some segments are omitted. (**b**) 'Oscillation' in segmentation of the mouse paraxial mesoderm. Oscillatory generation of new solitary travelling waves of expression of *HES/hairy* family genes, such as *HES1*, develops into a spatial periodic pattern[1,10–13]. The number at the peak of each wave indicates the birth order of the waves. (**c**) 'Insertion' of activator peaks, which has been observed in numerical simulations of reaction–diffusion systems of the activator-inhibitor type on a growing field[19–21]. Note that the new wave arises at a distance from the pre-existing waves. (**d**) 'Split' of activator peaks, which has been observed in numerical simulations of reaction–diffusion systems of the activator-depleted substrate type on a growing field[6,19,22,35]. Each cycle of splitting and shifting represents a kind of self-replication.

Results

Travelling of an *At-hh* stripe. To determine where the presumptive head ectoderm is located in the early stage 5-germ disc, we microinjected fluorescent dextran into single blastomeres. Tracking of labelled cell clones revealed that the head ectoderm corresponding to the Ch and Pp segments was derived from germ disc cells that had been located 3–5 cells away from the germ disc rim at early stage 5 (Fig. 2a,b). Live observation of a labelled cell clone followed by *in situ* hybridization revealed that the initial rim cells were internalized during mid-stage 5 to early stage 6, and many but not all of these cells became *At-twist* (*At-twi*)-expressing mesoderm cells[26,29] (Supplementary Fig. S1 and Supplementary Movie 1).

We examined the spatial relationships between the *At-hh* and *At-otd* expression patterns during early head development. The transcripts for *At-hh* and *At-otd* were co-expressed across 1–2 cells (in width) at the rim of the germ disc in early stage 5 (Fig. 2c). Despite cell internalization, *At-hh*- and *At-otd*-expression remained localized to the rim of the germ disc until the beginning of stage 6. Previous studies have found that as the germ disc begins to undergo morphological changes to form the germ band, the *At-hh* stripe shifts its relative position away from the anterior margin of the nascent germ band (the rim of the germ disc) towards the posterior (the centre of the germ disc)[23,27]. In the present study, double staining for *At-hh* and *At-otd* revealed that the shifting *At-hh* stripe was maintained at the posterior limit of the *At-otd* expression domain (Fig. 2d), which expands along the anteroposterior (AP) axis. Although this *At-hh* expression was considered dynamic in a previous study[23], the authors did not exclude the possibility that the relative shifting of the *At-hh* stripe may result from cell movement or cell recruitment.

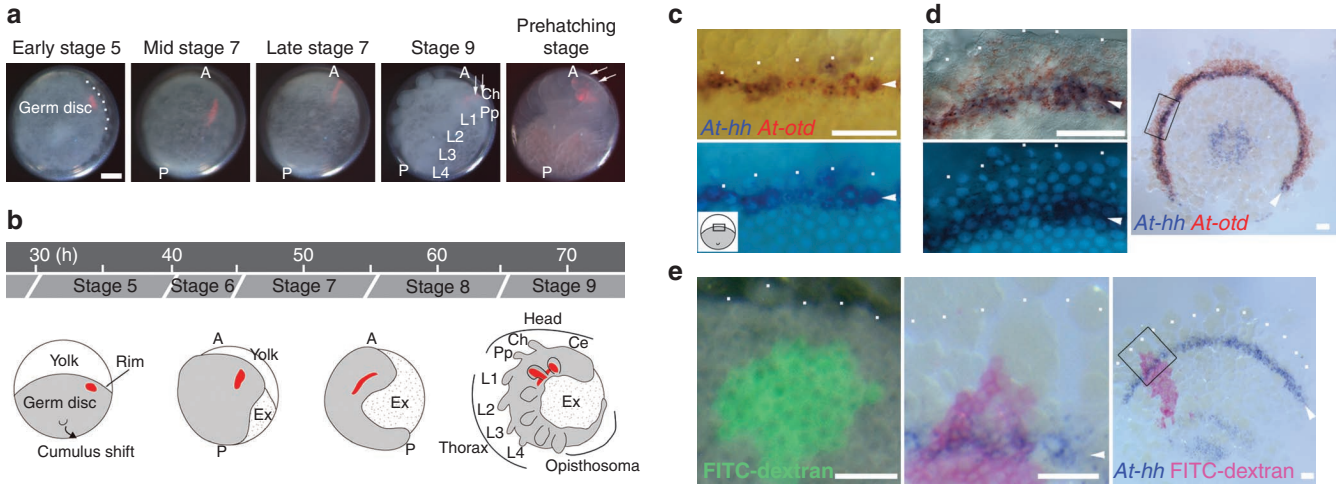

Figure 2 | Movement of the *At-hh* expression stripe from the rim of the germ disc. (**a**) Tracking of a small cell clone labelled by microinjection of RITC–dextran (red). The live embryo was photographed at stages indicated. The rim of the germ disc near the clone is dotted (early stage 5). Arrows indicate the developing Ch and Pp segments. (**b**) Schematic diagram of *Achaearanea* development highlighting the transformation of the germ disc into a segmented germ band. The tracked cell clone shown in **a** is depicted in red. Approximate time after egg laying is shown. (**c**) Expression of *At-hh* (purple) and *At-otd* (red) transcripts at early stage 5 at the rim of the germ disc (white dots). The lower panel shows the DNA fluorescence image. The inset contains an illustration of an embryo to show the orientation and the magnified region. (**d**) Expression of *At-hh* (purple) and *At-otd* (red) transcripts at mid-stage 6 in the anterior marginal region of the nascent germ band. Left panels are the magnified view of the boxed region in the right panel, and the lower one shows the DNA fluorescence image. White dots show the anterior margin. (**e**) Detection of an *At-hh* stripe in a tracked cell clone. An embryo having a cell clone labelled by FITC–dextran (green) more than two cells away from the rim of the germ disc (white dots) at early stage 5 (left panel) was fixed at early stage 7 and stained for *At-hh* transcripts (purple) and FITC–dextran (pink) (middle and right panels). The middle panel is a magnified view of the boxed region in the right panel. White dots show the anterior margin. Arrowheads indicate the *At-hh* stripe (**c**–**e**). Scale bars, 100 μm in **a**, 50 μm in **c**–**e**. A, anterior; Ce, cephalic lobe; Ch, chelicera; Ex, extraembryonic tissue; L, leg; P, posterior; Pp, pedipalp.

To examine the dynamic properties of the *At-hh*-gene-expression stripe, we used a combination of cell clone tracking and molecular staining. A labelled cell clone that had been more than two cells away from the germ-disc rim at early stage 5 was intersected by an *At-hh* stripe detected in the presumptive head ectoderm at early stage 7 (Fig. 2e). This result, together with the expression data presented above, suggested that, from early stage 5 to early stage 7, more central (or posterior) cells progressively began to express *At-hh*, and cells located at more peripheral (or anterior) positions, presumably including future mesoderm cells, stopped expressing *At-hh*. Thus, we concluded that, at least during stage 6, the *At-hh* stripe travels some distance posteriorly as a wave. However, it was not easy to determine when and where the posterior movement of the *At-hh* stripe stops, despite a gene expression boundary being formed between the head and thoracic regions (see below).

Repeated splitting of an *At-hh* gene expression stripe. To follow the fate of the travelling *At-hh* stripe in the spider-head ectoderm, we took advantage of the simultaneous development of sibling embryos within an egg sac. Embryos were fixed at intervals of 2 h from the beginning of stage 7 (the time point defined as 0 h) over a period of 10 h (up to early stage 8) and were then double-stained for *At-hh* and *At-otd* or *At-Deformed* (*At-Dfd*)[27] (Fig. 3). *At-Dfd* is a reliable marker of the thoracic region[30], and its expression domain was complementary to the *At-otd* expression domain at early stage 7, but not at stage 8 (Fig. 3a). At the 0-h time point, the *At-hh* stripe exhibited the form of an arched line ~2–4 cells wide that coincided with the posterior limit of the *At-otd*-expression domain, adjacent to the *At-Dfd*-expression domain (Fig. 3b–d). At the subsequent time points, the *At-hh* stripe overlapping with the *At-otd* expression domain broadened and nearly simultaneously or subsequently underwent insertion of an *At-hh*-negative domain, often exhibiting a pattern similar to an open mouth (Fig. 3b–d, 2, 4 h). Various transient patterns were observed among embryos fixed at the 2-h and 4-h time points (Supplementary Fig. S2), indicating that *At-hh* expression was disappearing from the middle regions of the stripe, a process that we refer to as 'splitting'. This splitting event was followed by shifting of the relative positions of the resulting stripes along the AP axis. Importantly, the anterior stripe remained *At-otd* positive, whereas the other stripe was *At-otd* negative. Only the *At-otd*-positive *At-hh* stripe underwent another cycle of splitting (Fig. 3b, 6–10 h). These two cycles of splitting of gene expression stripes, each of which took roughly 4 h, accounted for the three *At-hh* stripes observed later in the head ectoderm (Fig. 3b–d, 10 h), with the three stripes corresponding to the posterior portions of the Pp and Ch segments and the cephalic lobe (in this order starting from the posterior side).

Unlike in the head region, we observed no splitting pattern related to *At-hh* expression in the thoracic region. Three *At-hh* stripes of gene expression, corresponding to the L1-L3 segments, appeared nearly simultaneously from mid-stage 7 to early stage 8 (Fig. 3b,d, 8, 10 h). An *At-hh* stripe corresponding to the L4 segment formed at the posterior end of the *At-Dfd* expression domain in stage 6 (Fig. 3d, 0 h). The origins of the *At-hh* stripes for the opisthosomal segments seemed to be associated with the cycles of appearance and disappearance of *At-hh* expression at the centre of the caudal lobe (Fig. 3b,d). These observations imply that the mode of segmentation differs in the head, thoracic and opisthosomal regions. Furthermore, in contrast to *At-hh*, expression of another segment polarity gene homologue *At-engrailed* (*At-en*)[31], was first detected at mid-to-late stage 7 (Fig. 3e). This *At-en* stripe seemed to correspond to the L1 segment. In the head and opisthosomal regions, the initiations of *At-en* expression were much later than those of *At-hh* expression, suggesting that *At-en* is not involved in the early steps of spider-head segmentation.

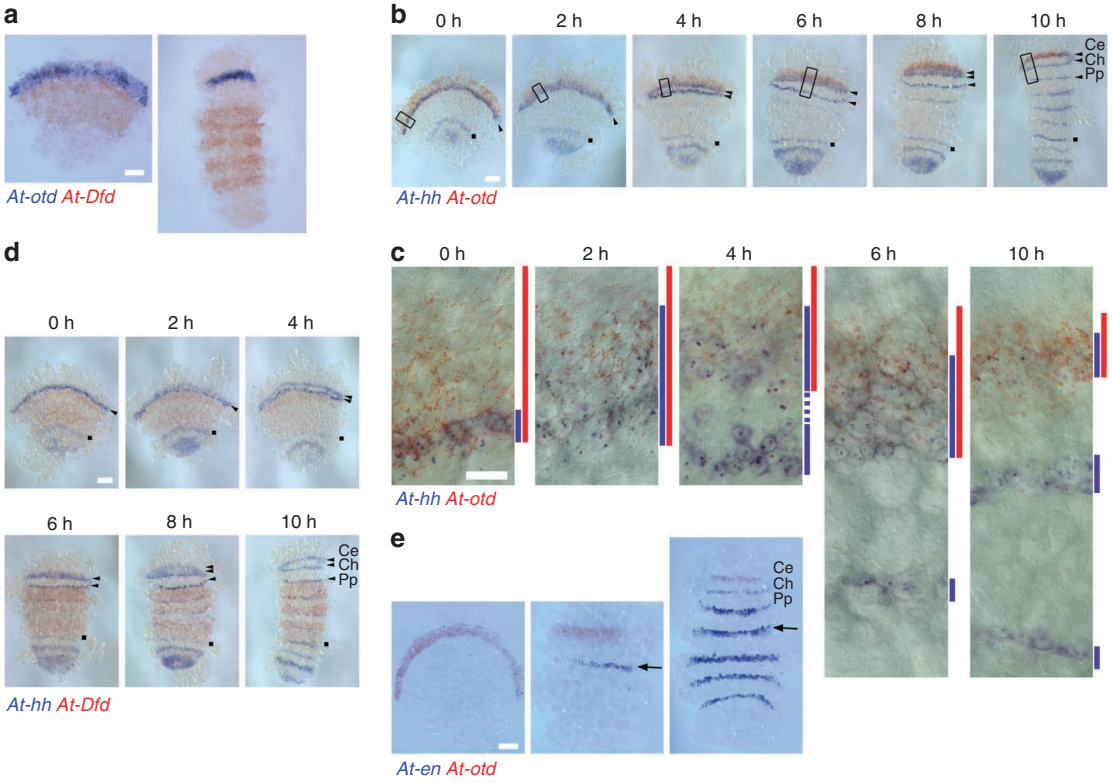

Figure 3 | Repeated splitting of the *At-hh* stripe associated with *At-otd* expression. (**a**) Comparison of the *At-otd* (purple) and *At-Dfd* (red) expression domains in embryos at early stage 7 (left) and stage 8 (right). (**b**) Embryos from a single egg sac that were fixed at 2-h intervals and stained for *At-hh* (purple) and *At-otd* (red). The first fixation was performed at early stage 7 (0 h). Arrowheads indicate *At-hh* stripes increasing in number in the presumptive head ectoderm. Dots indicate the *At-hh* stripe corresponding to the L4 segment. (**c**) Differential interference contrast images of the five regions boxed in **b**. Blue and red lines on the right of each panel indicate the ranges of the *At-hh* and *At-otd* expression domains, respectively. (**d**) Embryos from the same pools as in **b** stained for *At-hh* (purple) and *At-Dfd* (red) transcripts. The *At-hh* stripes are labelled in the same way as in **b**. (**e**) Embryos stained for *At-en* (purple) and *At-otd* (red) transcripts. Stage 6 (left), mid stage 7 (middle), and early stage 8 (right). Arrows indicate an *At-en* stripe that is likely to correspond to the L1 segment. All embryos are oriented anterior towards the top. Ce, cephalic lobe; Ch, chelicera; Pp, pedipal. Scale bars, 100 μm in **a**,**b**,**d**,**e**; 20 μm in **c**.

Stripe splitting is accompanied by convergent extension. To characterize the splitting process associated with the *At-hh* gene expression stripe in the head ectoderm at the cellular level, we monitored cell movements and cell divisions using live embryos locally expressing a fusion protein consisting of a nuclear localization signal (NLS) and tdEosFP (NLS-tdEosFP) ($n=4$). Photoconversion of tdEosFP facilitated cell tracking. We analysed a representative dataset that covered 14.5 h of development starting from late stage 5 (Fig. 4a,b; Supplementary Movie 2). This analysis revealed that a period of ~4.5 h (with few cell divisions) occurred between two 5-hr periods during which the cell number nearly doubled (Fig. 4c). During these three successive periods, the aspect ratio (length/width) of the labelled area progressively increased. Importantly, the cell counts across the width (the dorsoventral axis) of the labelled area decreased during the last two periods, indicating that oriented cell rearrangement in the epithelium contributed to elongating the AP axis of the head ectoderm, a typical convergent extension movement.

Furthermore, *in situ* hybridization following the live observation revealed that the monitored cell clone was intersected by two separate *At-hh* stripes of gene expression (Fig. 4b). Cell tracing in the time-lapse movie suggested that the cells that covered the two *At-hh* stripes at the last time point (14.5 h) came from a line of approximately two cell widths at the 0-h time point (corresponding to late stage 5) and a line of approximately four cell widths at the 5-h time point (corresponding to late stage 6) (Fig. 4a,b, circles) and, similarly, that the cells that comprised the *At-hh*-negative region between the *At-hh* gene expression stripes came from a line of approximately two cell widths at the 5-h time point (Fig. 4a,b, asterisks). At late stage 6, before entering the first splitting cycle, the *At-hh* stripe was usually observed as a line ~2–4 cell wide in essentially the same pattern as shown in Figure 3b–d, 0 h. These observations clearly show that the occurrence of an *At-hh*-negative domain between the two *At-hh* stripes during the splitting cycle is due to dynamic repression of *At-hh* expression accompanied by cell rearrangement in the surface epithelial layer, not by recruitment of *At-hh*-negative cells from other cell layers. We deduce from the time course of the development of the *At-hh* expression patterns (Fig. 3) that the timing of the first splitting event of the *At-hh* gene expression stripe corresponds to the second proliferative period (between the 9.5-h and 14.5-h time points). However, because locally enhanced rates of cell division were not observed (Fig. 4a,b; Supplementary Movie 2), it is unlikely that the expansion of the emerging *At-hh*-negative domain results from regulation of cell division patterns. It is technically difficult to determine when each stripe of *At-hh* expression is settled in lineage-restricted cell populations.

Role of *At-otd* for maintaining dynamic *At-hh* expression. In general, the use of parental RNA interference (pRNAi) has limitations in cases where knockdown of a target gene in the entire embryo prevents development at earlier stages than the developmental event

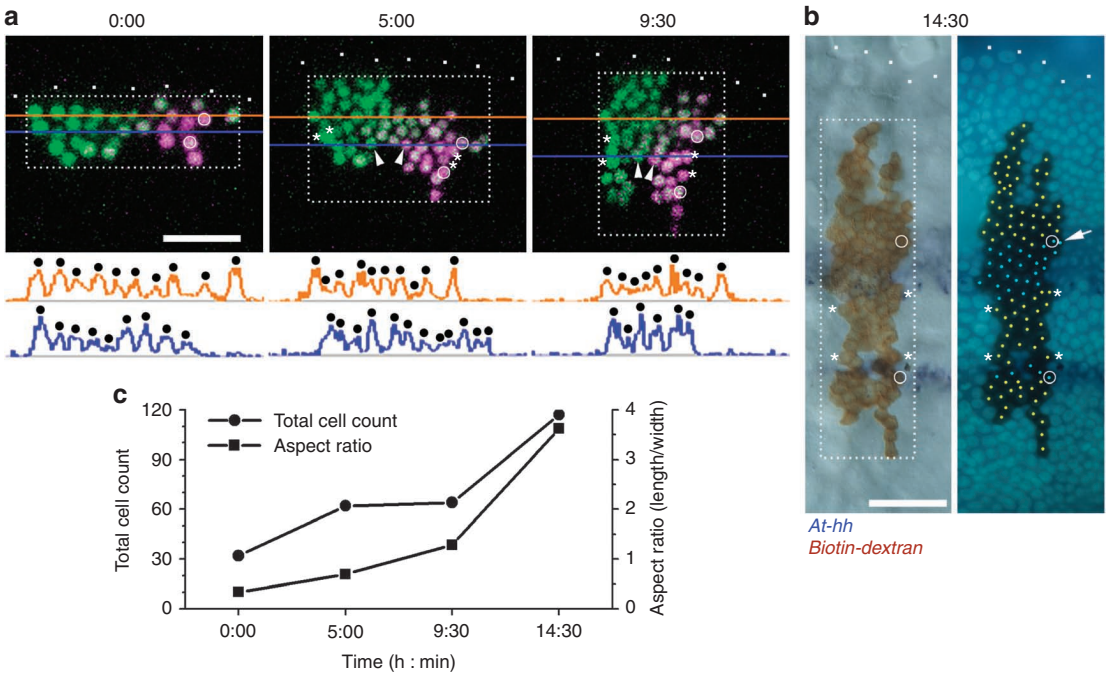

Figure 4 | Splitting of the head *At-hh* stripe in epithelium undergoing convergent extension. (**a**) Time-lapse observation of a cell clone expressing NLS-tdEosFP in the presumptive head ectoderm. The tdEosFP was photoconverted from the green (shown in green) to the red state (shown in purple) in a part of the cell clone just before time-lapse observation was performed, which started at late stage 5. A series of 10 optical sections (7.76 μm thickness) was collected every 10 min, and shown are projections of the optical sections collected at the times indicated (h:min). Arrowheads indicate two cells that were undergoing rearrangement to become adjacent to each other. Fluorescence intensity profiles along the orange and blue lines are shown below the photos to assist cell counting. (**b**) Detection of *At-hh* stripes in the observed embryo that was placed in the fixative at ~14:30, which was 10 min after the last images were collected. The left panel shows expression of *At-hh* transcripts (purple) and the cell lineage tracer biotin–dextran (brown), and the right shows the DNA fluorescence image. *At-hh*–positive and –negative cells in the labelled area are marked by light blue and yellow dots, respectively, although the signal was ambiguous in the cell indicated by the arrow. There were 22 labelled cells in the *At-hh*-negative domain between the two *At-hh* stripes. Asterisks indicate the cells at the corners of the *At-hh* negative region between the two *At-hh* stripes (**b**) and their ancestral cells (**a**), and circles indicate the cells at the anterior and posterior ends of the two stripes (**b**) and their ancestral cells (**a**). White dots indicate the anterior margin of the nascent germ band. Scale bars, 50 μm. (**c**) Graph showing changes in the total cell count and aspect ratio (length/width) for the rectangles shown in **a** and **b** of the labelled area.

of interest occurs. In a previous study[23], knockdown of *At-otd* by pRNAi was found to cause persistent localization of the *At-hh* stripe at the anterior margin of the nascent germ band. Here we observed that persistence of the *At-hh* stripe was concomitant with a failure in the normal specification of the *At-Dfd*-negative head region (Supplementary Fig. S3). In the case of *At-otd* pRNAi, it was impossible to investigate the role of *At-otd* during the travelling and splitting of the *At-hh* stripe.

To investigate the mechanisms underlying spider-head segmentation, we applied embryonic RNA interference (eRNAi) to *Achaearanea* embryos for the first time. Double-stranded RNAs (dsRNAs) for target genes, together with cell lineage tracers, were introduced into single blastomeres at the 32- to 128-cell stages. We confirmed that eRNAi produced cell-autonomous effects in *Achaearanea* with respect to the stability of target transcripts in the cytoplasm (Supplementary Fig. S4). Two different dsRNAs were prepared for each gene and microinjected to confirm the production of gene-specific phenotypes (Supplementary Table S1; Methods). The results obtained with only one of the two dsRNAs for each target gene are shown. In control eRNAi experiments, dsRNA for the jellyfish *green fluorescent protein* gene (*gfp*) was injected, which had no effects on the expression patterns of the target genes (Fig. 5a; Supplementary Fig. S5) or *At-hh*, regardless of the location of the cell clones into which the dsRNA was introduced (Fig. 5b; presumptive head ectoderm, $n = 12$ (including cell clones covering the germ disc rim, $n = 7$); thoracic and opisthosomal ectoderm, $n = 8$). In *At-otd* eRNAi experiments, when the dsRNA was introduced in the thoracic and opisthosomal regions, the *At-hh* expression patterns were not affected (Fig. 5c; $n = 7$). However, when the *At-otd* eRNAi cell clones covered the germ disc rim, similar, though local, defects compared with those caused by *At-otd* pRNAi were observed (Fig. 5d; 100%, $n = 7$). This finding is consistent with the suggestion that *At-otd* is not essential for the initiation of *At-hh* expression but is required for the relative shifting of the *At-hh* stripe in the anterior terminal region[23]. This local prevention of the movement of the *At-hh* stripe resulted in parallel progression of head segmentation in two separate regions without affecting the development of thoracic *At-hh* stripes (Fig. 5d). More importantly, when the *At-otd* eRNAi cell clones were located in the presumptive head ectoderm (slightly removed from the germ disc rim), the *At-hh* stripe was allowed to begin travelling but was broken into two adjacent stripes by the clones (Fig. 5e; 100%, $n = 10$). This unexpected phenotype was explained simply by loss of *At-hh* expression in the *At-otd* eRNAi cell clones. The separated *At-hh* stripes independently developed characteristic 'splitting' patterns with sizes adjusted to the smaller fields (Fig. 5e). Taken together, these results suggest that *At-otd* is required to maintain *At-hh* expression during the travelling and splitting phases and that the *At-otd*-positive *At-hh* stripe serves as a generative zone for the spider-head segments.

Moreover, phenotypes similar to those obtained from *At-otd* eRNAi were produced by performing eRNAi against *At-cubitus*

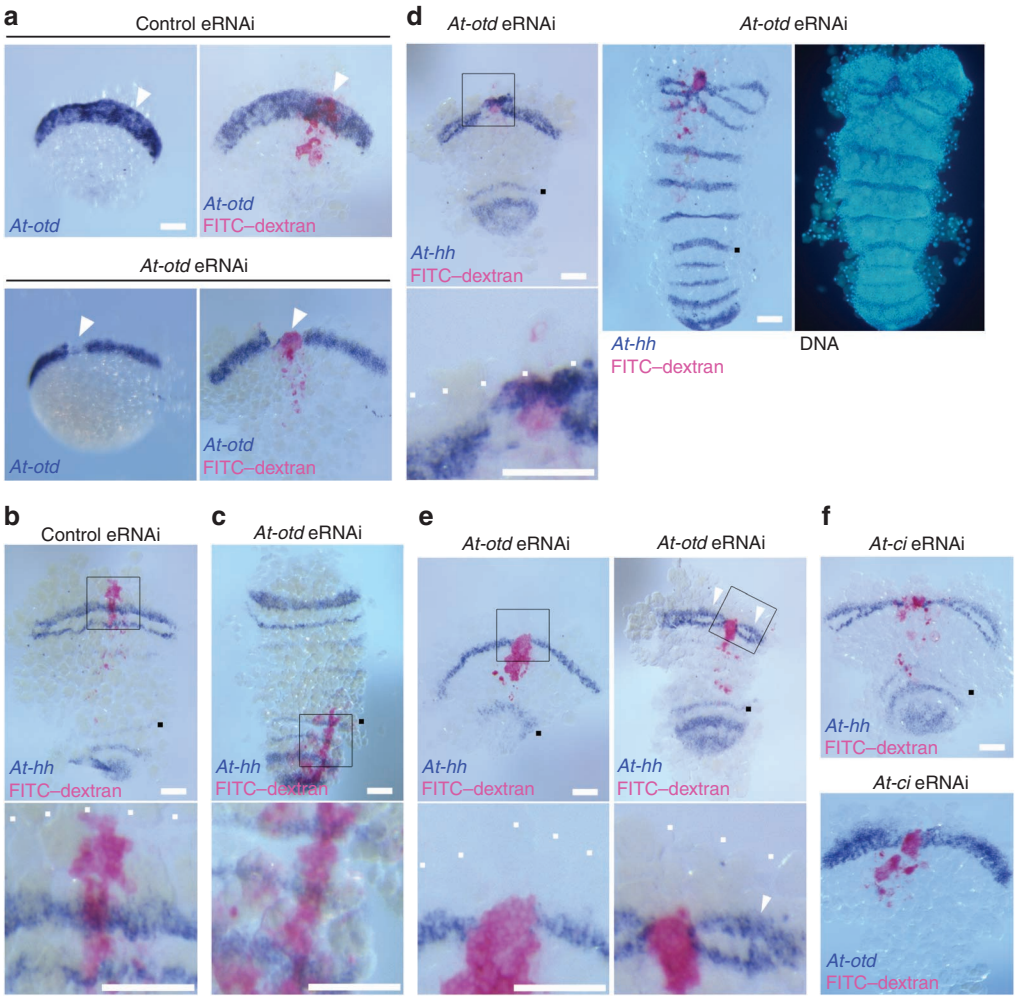

Figure 5 | *At-otd* activity is required to maintain dynamic *At-hh* expression in the presumptive head ectoderm. (**a**) Detection of *At-otd* transcripts in embryos microinjected with control *gfp* dsRNA (upper panels) and *At-otdXE* dsRNA (lower panels). Each embryo was photographed before (left) and after (right) staining for the lineage tracer FITC-dextran (pink). Arrowheads indicate areas where the lineage tracer and presumably the dsRNAs were introduced. (**b**) Control (*gfp*) eRNAi embryo stained for *At-hh* transcripts (purple) and the cell-lineage tracer FITC-dextran (pink), which was detected in the presumptive head ectoderm. Embryos shown in the following panels were stained in the same way as this embryo, unless otherwise indicated. (**c**) *At-otd* eRNAi embryo in which the labelled cell clone (pink) extended from the L4 segment to the caudal lobe. (**d**) Two *At-otd* eRNAi embryos that experienced having a labelled clone (pink) at the anterior margin of the nascent germ band at stages 6 and 7. The embryo in the left panel was fixed at stage 7, and that in the middle and right was allowed to develop until stage 8 and fixed for staining. The right panel shows the DNA fluorescence image. (**e**) *At-otd* eRNAi embryos in which the labelled clone (pink) was slightly removed from the anterior margin (white dots). The right embryo was slightly older than the left one. Arrowheads in the right panel indicate the adjacent *At-hh* stripes that each exhibited a characteristic splitting pattern with sizes adjusted to the fields. (**f**) *At-ci* eRNAi embryos; the lower one was stained for *At-otd* transcripts (purple) and the cell-lineage tracer FITC-dextran (pink). All embryos in this figure were at germ band-forming stages (corresponding to stage 7) except the embryo in right and middle panels of **d**, which was at stage 8. Boxed areas in the upper panels are magnified in the lower panels (**b**,**c**,**e**, left column of **d**). White dots indicate the anterior margin (**b**,**d**,**e**), and black dots indicate the *At-hh* stripe at the L4 segment (**b**–**f**). Scale bars, 100 μm.

interruptus (*At-ci*) (Fig. 5f; 100%, $n=8$ for clones covering the germ disc rim and $n=7$ for clones removed from the germ disc rim in the presumptive head region), a homologue of *Drosophila ci* (Supplementary Fig. S6), which encodes a transcription factor that mediates the transduction of Hh signalling[32]. In *At-ci* eRNAi cell clones, *At-otd* expression was abrogated or greatly reduced (Fig. 5f; 100%, $n=12$). These results suggest that *At-hh* activity promotes *At-otd* expression via *At-ci*, while the *At-otd* activity promotes *At-hh* expression to maintain the head generative zone.

Role of another Hh signalling target for promoting splitting. To identify targets of Hh signalling other than *At-otd*, we carried out a microarray-based screen for genes that were downregulated in *At-hh* pRNAi embryos at late stage 5 (Supplementary Table S2). A homologue of the *Drosophila* pair-rule gene *odd-paired* (*opa*)[33], *At-opa* (Supplementary Fig. S6), emerged as a putative target of Hh signalling in this screen. *At-opa* transcripts were detected in a broad marginal region of the germ disc covering the presumptive head ectoderm at late stage 5 (Fig. 6a); consistent with the microarray data, this expression was missing in *At-hh* pRNAi embryos (Fig. 6a). Later, relatively strong expression of *At-opa* transcripts was persistently observed at and near the *At-otd*-positive *At-hh* stripe, whereas weaker levels of stripe expression appeared in forming germ bands (Fig. 6b; Supplementary Fig. S7). pRNAi against *At-opa* caused a delay in axial elongation and simultaneously impaired the splitting of the head *At-hh* stripe without disrupting

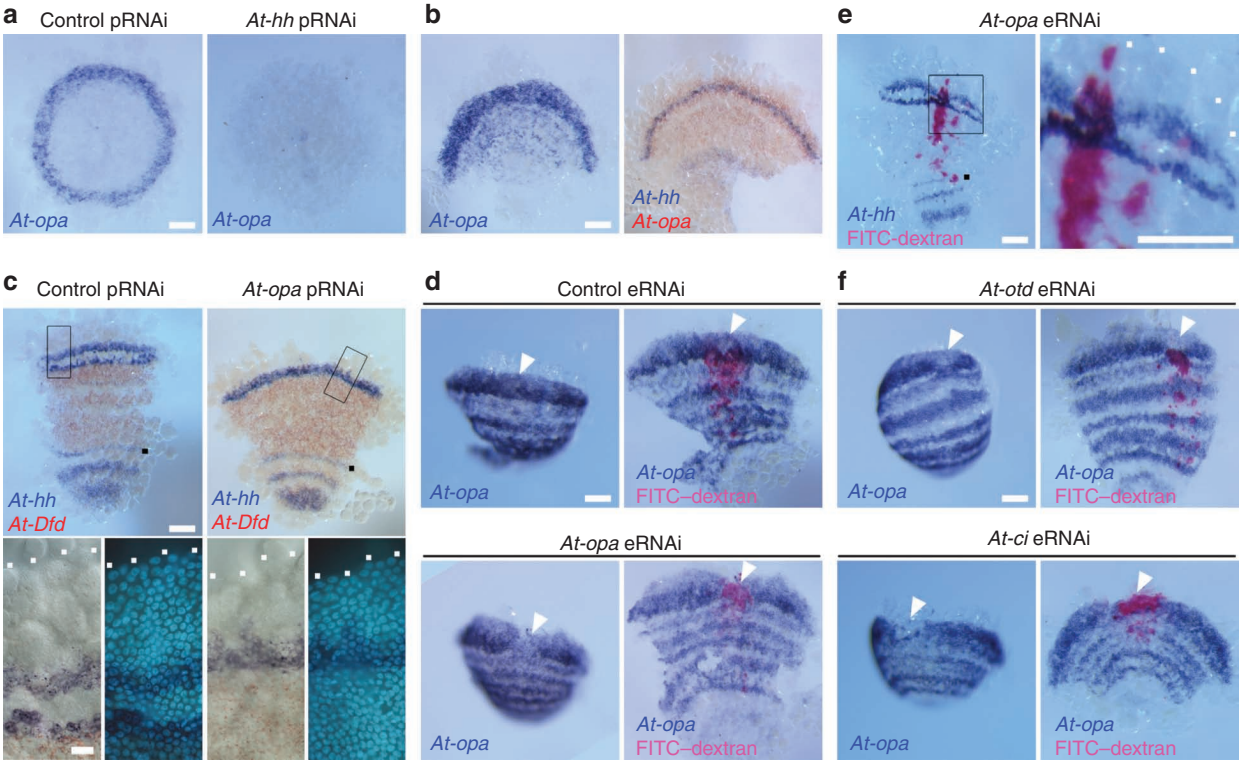

Figure 6 | *At-opa* activity is required to promote stripe splitting and its expression is regulated by segmentation genes. (**a**) Control (*gfp*) (left) and *At-hh* (right) pRNAi embryos at late stage 5 stained for *At-opa* transcripts. (**b**) Embryos at early stage 7 single-stained for *At-opa* transcripts (left) and double-stained for *At-hh* (purple) and *At-opa* (red) transcripts (right). (**c**) Control (*gfp*) (left) and *At-opa* (right) pRNAi embryos at germ band-forming stages stained for *At-hh* (purple) and *At-Dfd* (red) transcripts. The boxed areas in the upper panels are magnified in the lower panels; the right ones are fluorescence images of DNA staining. The right embryo is ~6 holder than the left embryo (see Methods). Note that the number of *At-hh* stripes for the L4 (black dots) and more posterior segments is an alternative indicator of developmental stage. (**d**) Detection of *At-opa* transcripts in embryos microinjected with control *gfp* dsRNA (upper panels) and *At-opaF* dsRNA (lower panels). Each embryo was photographed before (left) and after (right) staining for the lineage tracer FITC–dextran (pink). Arrowheads indicate areas where the lineage tracer and, presumably, the dsRNAs were introduced. (**e**) *At-opa* eRNAi embryo stained for *At-hh* transcripts (purple) and the cell lineage tracer FITC–dextran (pink). The boxed area in the left panel is magnified in the right panel. (**f**) Detection of *At-opa* transcripts in *At-otd* eRNAi (upper panels) and *At-ci* eRNAi (lower panels) embryos. Staining and photographing were performed in the same way as in **d**. White dots indicate the anterior margin of the germ band, and black dots indicate the *At-hh* stripe in the L4 segment (**c**,**e**). Embryos shown in **d**–**f** were at early or mid stage 7. Scale bars, 20 μm in the lower panel of **c**, 100 μm in other panels.

the travelling process or the anterior terminal patterning (Fig. 6c; Supplementary Fig. S3). This situation resembles what is seen during *Drosophila* pair-rule patterning, which is coupled with convergent extension[34]. A similar delay in axial elongation was also observed in *At-otd* pRNAi embryos (Supplementary Fig. S3).

To more directly investigate the role of *At-opa* in head segmentation, we used eRNAi (Fig. 6d). In *At-opa* eRNAi cell clones located in the presumptive head ectoderm, the *At-hh* stripe was prevented from splitting (Fig. 6e; 90%, $n=10$). These results suggest that *At-opa* activity promotes stripe splitting in the head generative zone.

Regulation of *At-opa* striped pattern formation. To investigate the role of *At-otd* in the regulation of *At-opa* expression, we examined *At-otd* eRNAi cell clones. In cell clones located in the thoracic and opisthosomal region, *At-opa* expression was not affected ($n=8$). In contrast, in cell clones located in the presumptive head ectoderm, the levels of *At-opa* expression were considerably reduced, and the head *At-opa* stripes failed to separate (Fig. 6f; 90%, $n=10$), suggesting that *At-otd* activity is required in the presumptive head ectoderm for normal development of the striped pattern of *At-opa* expression. Similar phenotypes were observed in *At-ci* eRNAi cell clones located in the presumptive head ectoderm (Fig. 6f; 100%, $n=11$). Furthermore, depletion of *At-opa* transcripts by *At-opa* pRNAi resulted in a uniform pattern of *At-opa* transcription (Supplementary Fig. S8). This suggests that the activity of *At-opa* is required for its striped pattern of transcription to be established.

Discussion

We have identified the splitting of gene expression stripes as a mode of segmentation in *A. tepidariorum* that occurs in the presumptive head ectoderm using microinjection-based techniques, such as cell labelling and eRNAi. This segmentation type presents several unique features compared with *Drosophila* blastoderm subdivision and vertebrate oscillatory segmentation (Compare Fig. 7 with Fig. 1a,b). First, movement of a gene expression wave is a critical step in specifying the segmentation field. This was suggested by the observation that stripe-travelling defects caused by *At-otd* pRNAi (ref. 23; Supplementary Fig. S3) and eRNAi (Fig. 5d) were followed by failures in the formation of the head region. Second, there is a narrow (stripe-shaped) generative zone from which new repetitive units form in a specific sequence. Segmentation in this zone would resemble those in the presomitic mesoderm of vertebrate embryos and the posterior growth zone of short-germ arthropod embryos in that they show temporal repetition. Third, development of segmental gene expression patterns is associated with convergent extension elongating the tissue axis. Fourth, the changing patterns of gene

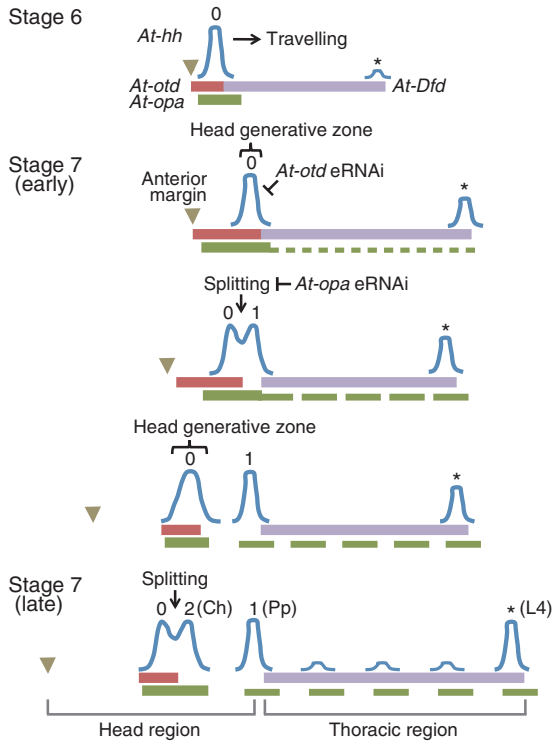

Figure 7 | Schematic illustrations showing the changes in gene expressions involved in *Achaearanea* head segmentation. The expression domains of *At-hh* (blue waves), *At-otd* (brown boxes), *At-opa* (green boxes), and *At-Dfd* (purple boxes) along the AP axis at five successive stages of development are illustrated. Only the head and thoracic regions are shown. The *At-otd*-positive wave of *At-hh* expression, marked by '0', is defined as the generative zone for the Pp and Ch segments, which form by stripe splitting in that order and are indicated by '1' and '2', respectively. The anterior margin of the forming germ band (closed triangles) and the *At-hh* expression stripe related to the L4 segment (asterisks) are also indicated. *At-otd* eRNAi inhibits *At-hh* expression in the head generative zone, and *At-opa* eRNAi prevents the *At-otd*-positive *At-hh* stripe from splitting. In earlier stages (late stage 5 and early stage 6), *At-otd* eRNAi inhibits the departure of the *At-hh* stripe from the rim of the germ disc, but this fact is not shown.

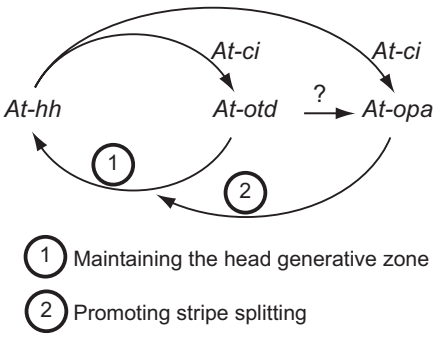

Figure 8 | A model for mechanisms underlying spider-head segmentation. An autoregulatory signalling network in which *At-hh*, *At-ci*, *At-otd*, and *At-opa* participate is proposed. Expression of *At-otd* and *At-opa* is controlled by short- and longer range activities of *At-hh*, respectively, via *At-ci*, and activities of *At-otd* and *At-opa* are required for the dynamic regulation of *At-hh* expression during head segmentation. *At-otd* activity mediates positive feedback to maintain the head generative zone, and *At-opa* activity promotes the *At-hh*—*At-otd* circuit to enter the splitting phase through an as yet unknown mechanism in the head generative zone. The stripe splitting may involve coordinated regulation of gene expression and cell rearrangement. *At-otd* may directly and/or indirectly regulate levels of *At-opa* expression and the development of its pattern.

expression involved in segmentation mimic the travelling and peak splitting of waves that have been observed in numerical simulations of a class of autocatalytic reaction–diffusion systems in a growing field (Fig. 1d). 'Stripe splitting', a behaviour similar to self-replication (Fig. 1d), is distinguished from the oscillatory generation of new waves in the terminal region (Fig. 1b) and from the insertion of new waves at a distance from pre-existing waves (Fig. 1c). On the basis of these observed features, we suggest that spider-head segmentation is of particular importance in understanding the relationships among the diverse modes of animal segmentation, and we categorize it as the split-type segmentation.

Here we have characterized some of the molecular mechanisms associated with spider-head segmentation. Taken together with the results of our previous study[27], these findings suggest that Hh signalling has central roles in AP axis formation and subsequent head segmentation. We found that although expression of *At-otd* and *At-opa* is controlled by Hh signalling via *At-ci*, their activities are required to dynamically regulate the distribution patterns of Hh-signalling sources. These findings led us to propose that spider-head segmentation requires an autoregulatory signalling network in which *At-hh*, *At-ci*, *At-otd* and *At-opa* participate (Fig. 8). It is important to note that the posterior limit of the *At-otd* expression domain continues to be closely associated with the anterior-most *At-hh* stripe (Figs 3b,c and 7), suggesting that *At-otd* transcription is activated by short-range activity of Hh signalling. In contrast, at least at late stage 5 and late stage 6 (Figs 6a,b and 7), the posterior limit of the broad *At-opa*-expression domain is away from the *At-hh*-signalling source, suggesting that *At-opa* transcription is activated by longer range signals. Positive feedback regulation of Hh signalling by *At-otd* seems to contribute to maintaining the spider-head generative zone, whereas *At-opa*, encoding a Zic family transcription factor, may be a key gene required to generate stripe-splitting dynamics in the head generative zone.

Peak splitting of gene expression waves has been characteristically observed in numerical simulations of activator-depleted substrate systems, which assume local self-enhancement (autocatalysis) and depletion of a substance required for the self-enhancement[6,35]. The *At-hh*—*At-otd* reciprocal positive regulation might mimic local self-enhancement, whereas *At-opa* may act as a cofactor involved in the self-enhancement. If the At-Opa protein is consumed, depletion of this product might promote the *At-hh*—*At-otd* circuit to enter the splitting phase. With respect to this possibility, mammalian Zic proteins may act synergistically with Gli proteins, which are Ci homologues, to enhance the transduction of Hh signalling[36]. Zic and Gli family proteins share a highly conserved zinc finger domain (Supplementary Fig. S6) and have cooperative roles in multiple developmental processes[37,38]. Alternatively, the At-Opa product might have a substantial inhibitory effect on Hh signalling preferentially at sites where its signalling activities are saturated. Zic family proteins also act antagonistically with Gli family proteins[36]. These hypotheses need to be tested.

An important aspect of our findings is that the observed splitting of gene expression stripes may require coordinated regulation of gene expression and cell rearrangement. Knockdown of *At-otd* and *At-opa* appeared to delay convergent extension. *At-otd* and *At-opa* activities may mediate interactions of multiple signalling pathways that coordinate pattern formation and cell movements. The types of signalling pathways, other than Hh signalling, involved in this gene expression stripe splitting are a key issue to be studied in the future.

Identification of shared genetic components suggests an evolutionary link between spider stripe-splitting segmentation and *Drosophila* Bicoid-based segmentation. The proposed autoregulatory signalling network for the stripe-splitting segmentation contrasts with the hierarchical cascades of maternal, gap and pair-rule genes associated with *Drosophila* blsastoderm subdivision while sharing Hh-signalling components with the segment polarity network. The activities of the *Drosophila* pair-rule genes prepattern the segments and activate the segment polarity gene network[17], in which the Hh and Wingless signalling pathways have reciprocal regulatory interactions to determine correct cell fates within each segment[39,40]. Importantly, roles of these signalling pathways are restricted to the terminal steps in *Drosophila* segmentation. Curiously, the gene expression stripe splitting is somewhat similar to pair-rule patterning that has been observed in some short-germ arthropod embryos, where domains of gene expression are progressively resolved into segmental stripes[23,24]. Our findings and these facts may provide hints about the evolution of mechanisms of pair-rule patterning. Mutations affecting network structures of segmentation genes could have led to diversification of strategies for arthropod segmentation[4]. As mentioned above, the spider embryo exhibits at least three distinct modes of segmentation depending on the body part. Intriguingly, *Drosophila* subdivision is achieved by distinct mechanisms in the head and trunk regions[3,41,42]. Increases in the number of stripes or patches of segment polarity gene homologue expression have been observed in the developing head region of *Drosophila* and other arthropod embryos[43–47], where split-like patterning events may occur. Furthermore, the spider-head generative zone is analogous to the vertebrate midbrain–hindbrain boundary zone, which is considered the head organizer, in which both zones are defined by the posterior limits of the expression domains of the *otd*/*otx* homologues[48]. Animal segmentation will continue to be a challenging subject in studying how developmental strategies diversified during animal body plan evolution.

Methods

Spiders. This work was performed according to institutional animal care and use committee guidelines. Laboratory stocks of the house spider *A. tepidariorum* were maintained at 25 °C. The development of sibling embryos was monitored to evaluate the quality of the embryos used in our experiments. Developmental stages were described previously[25,28,29].

Embryo staining. Embryos from a single egg sac were fixed at 2-h intervals from the beginning of stage 7 and pooled as a series of 0 h to 10 h samples. Embryos shown in Figures 3b–d and 6b, and Supplementary Figures S2 and S7 were derived from this series. Embryo fixation and whole-mount *in situ* hybridization were performed, as described previously[28,31]. Fluorescein isothiocyanate (FITC)–dextran in fixed samples was visualized using an alkaline phosphatase-conjugated sheep anti-FITC antibody (1:1000, dilution; Roche) and the Vector Red substrate (Vector). Biotin–dextran was visualized using the VECTASTAIN Elite standard ABC kit (Vector). Most samples were counterstained with 4′,6-diamidino-2-phenylindole (DAPI; Sigma-Aldrich). Embryos were examined using an SZX12 fluorescence stereomicroscope (Olympus) equipped with a colour charge-coupled device camera (C7780-10; Hamamatsu Photonics) and/or an Axiophot2 fluorescence microscope equipped with differential interference contrast optics (Carl Zeiss).

Microinjection. Embryos at appropriate stages were dechorionated with commercial bleach, placed on glass slides, covered with halocarbon oil 700 (Sigma), and subjected to microinjection as described[25]. A 1 μg μl^{-1} solution of FITC–dextran (MW 500,000, Sigma-Aldrich) or rhodamine B isothiocyanate (RITC)–dextran (MW 70,000, Sigma-Aldrich) was injected into 32- to 128-cell stage embryos. Live embryos were photographed using the fluorescence stereomicroscope.

Plasmid construction and mRNA preparation. The pSP64 poly(A) vector (Promega) was modified to replace the *Eco*RI site after the poly A sequence with a *Not*I site. This plasmid was designated pSP64-polyA-NotI+. A blunt-ended *Xho*I-*Bam*HI fragment of the pcDNA3-Flag1-td-EosFP plasmid (Molecular Biotechnology) was inserted into the *Sma*I site of pSP64-polyA-NotI+ to produce pSP64-tdEosFP-polyA-NotI+. A *Hind*III (blunt-ended)-*BamHI* fragment encoding the NLS (the amino acid sequence, MAKIPPKKKRKVED) was inserted between the *Hinc*II and *Bam*HI sites of pSP64-tdEosFP-polyA-NotI+. The resulting plasmid was designated pSP64-NLS-tdEosFP-polyA-NotI+ and was cut with *Not*I for use as a template for *in vitro* transcription. Capped sense messenger RNA was synthesized using the mMESSAGE mMACHINE SP6 Kit (Ambion) according to the manufacturer's instructions.

Time-lapse observations. Embryos at the 32-cell stage were injected with a mixture of *NLS-tdEosFP* mRNA (0.25 μg μl^{-1}). and biotin–dextran (MW 70,000, Sigma-Aldrich, 1.0 μg μl^{-1}). For photoconversion of tdEosFP, small areas of the embryos were ultraviolet irradiated for less than 3 min under the Axiophot2 fluorescence microscope using a band-pass excitation filter (Chroma No. 31022, BP 395±20) and a X40 objective. Neither the expression of NLS-tdEosFP nor the ultraviolet irradiation resulted in any detectable toxic effect on development. Time-lapse microscopy was performed using the TCS SPE confocal system (Leica). Images were processed using Leica LAS-AF ver. 2.21, ImageJ ver. 1.44 (NIH) and Adobe Photoshop CS2 software.

Microarray-based screen of spider genes. We obtained 22,812 expressed sequence tags (ESTs) sequenced from the 5′ end from five complementary DNA (cDNA) libraries of *A. tepidariorum* embryos. These sequences were deposited in the DNA Data Bank of Japan under accession numbers FY216297–FY225483 and FY368221–FY381845. To design microarray probes, 13,655 non-redundant sequences were selected from the EST data. Using these sequences and a few extra sequences, 40 mer oligonucleotide probes were designed using OligoArray 2.1 software[49] and embedded in CombiMatrix custom microarrays (12K×2). Total RNA was extracted from two different populations of late-stage 5 embryos derived from different egg sacs produced by a single female 1 day before (normal) and 20 days after (*At-hh* pRNAi) the first injection of *At-hh1* dsRNA. This female was given a total of four injections of ~1.5 μl of *At-hh1* dsRNA solution (2 μg μl^{-1}) at 2–3 day intervals. cRNA labelled with Cy3 (normal) or Cy5 (*At-hh* pRNAi) was prepared from 2 μg of total RNA using the RNA Transcript SureLABEL Core Kit (TaKaRa). cRNA probes were hybridized to microarrays in hybridization buffer (5× saline-sodium citrate buffer, 0.1% sodium dodecyl sulphate, 10% formamide) at 42 °C for 16–20 h. Microarray slides were scanned using a GenePix 4000B Scanner (Molecular Devices), and the obtained images were analysed using Array-Pro Analyzer version 4.5 (Media Cybernetics). The quantitative data were subjected to loess normalization. To validate this microarray experiment, probes for *At-hh* and *At-otd* served as positive controls; probes for an *α-catenin* homologue, an elongation factor *1α* homologue, and an *H3 histone* homologue were used as negative controls (Supplementary Table S2). The intensity ratio values in the spots for two EST clones representing sequences homologous to *Drosophila opa*, eS6_d1_54_H12 (FY376203) and eS7_SB_031_C08 (FY380182) were as low as those for the positive controls. These EST clones were clustered with another EST clone At_eW_022_A24 (FY223306). The microarray dataset was deposited in the Gene Expression Omnibus database under accession number GSE26468.

cDNA and genomic DNA cloning. The EST clone At_eW_022_A24 and an extra cDNA clone obtained by 5′ rapid amplification of cDNA ends (RACE) were used to determine the sequence of the entire coding region of *At-opa*. A short sequence homologous to *Drosophila ci* was originally found in an EST clone eS6_d1_31_A04 (FY374226). A full-length cDNA clone for *At-ci* was obtained by 5′ and 3′ RACE and cDNA library screening. Analyses with BLASTP and Mega version 4.0 (ref. 50) confirmed that the predicted proteins encoded by *At-opa* and *At-ci* were zinc finger proteins that belong to the Opa/Zic and Ci/Gli subfamilies, respectively (Supplementary Fig. S6). cDNA clones covering the entire coding region of an *A. tepidariorum* homologue of *six3*, designated *At-six3-1*, were obtained by PCR using degenerate primers and 5′ and 3′ RACE. The sequences are available from the DNA database of Japan under the accession numbers *At-opa*, AB605264; *At-ci*, AB605263; and *At-six3-1*, AB605265.

A genomic DNA clone sharing a sequence with the *At-opa* cDNA clone was obtained by screening an *A. tepidariorum* genomic library (λdash II) constructed during this study. This clone covered at least a part of an intron following an exon/intron boundary that is evolutionarily conserved at the junction of the zinc finger 3 and 4 coding regions[51]. A 1-kb fragment within this intron was used to prepare an intron probe to detect *At-opa* pre-mRNA.

RNAi. DNA templates for dsRNA synthesis were prepared by PCR with primers bearing the T7 or Sp6 promoter sequence. dsRNA was synthesized using a MEGAscript kit (Ambion) as described[52]. *gfp* dsRNA was used as a control. To validate the specificity of the RNAi effects, we prepared two different dsRNAs per gene, which were derived from non-overlapping regions of the cDNA or regions with a minimum overlap (four nucleotides). For *At-otd* and *At-opa* RNAi, longer dsRNAs were also prepared and tested to confirm the consistency of the results. Information on the dsRNAs used in this study is summarized in Supplementary Table S1. Reduced expression levels of the target transcripts were confirmed by *in situ* hybridization and/or quantitative reverse transcription polymerase chain reaction (Supplementary Table S1).

pRNAi was performed by injecting dsRNA into the opisthosoma of females using a pulled glass capillary, as described in ref. 31. Individual females were given multiple injections of 1.5–2.0 μl of a dsRNA solution (2 μg μl^{-1}) at 2- to 3-day intervals (*At-opa1*, *At-opaF*, *At-otd1*, *At-otdXE*, *At-hh1* and *At-hh2* dsRNAs, four or five injections; *At-opaH* and *gfp* dsRNAs, seven injections). *At-opa* pRNAi

and *At-otd* pRNAi reduced the speed of the transition from the germ disc to the germ band. To exclude the possibility that the defects described for these pRNAi embryos resulted from developmental delays, we examined these embryos at slightly later stages than the control embryos. The embryos shown in Figure 6c (right) and Supplementary Figure S3a,d,f were ~6 h older than the control embryos shown in Figure 6c (left) and Supplementary Figure S3e,g.

In the eRNAi experiments, a mixture of dsRNA (0.3–0.4 $\mu g\,\mu l^{-1}$) and FITC–dextran (0.4–0.8 $\mu g\,\mu l^{-1}$) or a mixture of dsRNA (0.4 $\mu g\,\mu l^{-1}$) and RITC-dextran (0.8 $\mu g\,\mu l^{-1}$) plus biotin–dextran (MW 10,000, Sigma-Aldrich, 0.4 $\mu g\,\mu l^{-1}$) (for the experiment shown in Supplementary Fig. S4) was microinjected into 32- to 128-cell stage embryos. At the time of injection, the fates of the injected cells were not predictable because of the spherical symmetry of the early *Achaearanea* embryo. At late stage 5, morphologically normal embryos in which labelled cell clones were located at target sites of the germ disc epithelium were selected under the fluorescence microscope for analysis. As it was not possible to strictly control the injection volume, the amount of dsRNA incorporated into embryonic cells (as indicated by the fluorescence intensity of incorporated FITC–dextran) slightly varied from embryo to embryo. However, such variations had little effect on the experimental results.

In the pRNAi and/or eRNAi experiments for each gene, the same results were independently obtained with the two dsRNAs. The results shown here were obtained with one of the dsRNAs for each gene: *At-opaF*, *At-otdXE*, *At-ci1*, and *At-hh1* (against *At-opa*, *At-otd*, *At-ci*, and *At-hh*, respectively). In the eRNAi experiments, we obtained the same results in 80% or more of embryos examined ($n \geq 5$) with the other dsRNA for each gene.

References

1. Dequéant, M. L. & Pourquié, O. Segmental patterning of the vertebrate embryonic axis. *Nat. Rev. Genet.* **9,** 370–382 (2008).
2. Peel, A. D., Chipman, A. D. & Akam, M. Arthropod segmentation: beyond the *Drosophila* paradigm. *Nat. Rev. Genet.* **6,** 905–916 (2005).
3. Tautz, D. Segmentation. *Dev. Cell* **7,** 301–312 (2004).
4. Fujimoto, K., Ishihara, S. & Kaneko, K. Network evolution of body plans. *PLoS One* **3,** e2772 (2008).
5. Baker, R. E., Schnell, S. & Maini, P. K. Mathematical models for somite formation. *Curr. Top. Dev. Biol.* **81,** 183–203 (2008).
6. Meinhardt, H. *Models of Biological Pattern Formation*, Academic Press, 1982.
7. Cooke, J. & Zeeman, E. C. A clock and wavefont model for control of the number of repeated structures during animal morphogenesis. *J. Theor. Biol.* **58,** 455–476 (1976).
8. Pankratz, J. A. & Jäckle, H. in *The Development of Drosophila melanogaster* (eds Bate, M. & Martinez-Arias, A.) Vol. I, 467–516 (Cold Spring Harbor, 1993).
9. Lawrence, P. A. *The Making of a Fly: The Genetics of Animal Design*, Blackwell Scientific, 1992.
10. Masamizu, Y. *et al.* Real-time imaging of the somite segmentation clock: revelation of unstable oscillators in the individual presomitic mesoderm cells. *Proc. Natl Acad. Sci. USA* **103,** 1313–1318 (2006).
11. Bessho, Y., Hirata, H., Masamizu, Y. & Kageyama, R. Periodic repression by the bHLH factor Hes7 is an essential mechanism for the somite segmentation clock. *Genes Dev.* **17,** 1451–1456 (2003).
12. Jouve, C. *et al.* Notch signalling is required for cyclic expression of the hairy-like gene HES1 in the presomitic mesoderm. *Development* **127,** 1421–1429 (2000).
13. Palmeirim, I., Henrique, D., Ish-Horowicz, D. & Pourquié, O. Avian *hairy* gene expression identifies a molecular clock linked to vertebrate segmentation and somitogenesis. *Cell* **91,** 639–648 (1997).
14. Stollewerk, A., Schoppmeier, M. & Damen, W. G. Involvement of *Notch* and *Delta* genes in spider segmentation. *Nature* **423,** 863–865 (2003).
15. Lewis, J. Autoinhibition with transcriptional delay: a simple mechanism for the zebrafish somitogenesis oscillator. *Curr. Biol.* **13,** 1398–1408 (2003).
16. Jaeger, J. *et al.* Dynamic control of positional information in the early *Drosophila* embryo. *Nature* **430,** 368–371 (2004).
17. von Dassow, G., Meir, E., Munro, E. M. & Odell, G. M. The segment polarity network is a robust developmental module. *Nature* **406,** 188–192 (2000).
18. Bodnar, J. W. Programming the *Drosophila* embryo. *J. Theor. Biol.* **188,** 391–445 (1997).
19. Crampin, E. J., Hackborn, W. W. & Maini, P. K. Pattern formation in reaction-diffusion models with nonuniform domain growth. *Bull. Math. Biol.* **64,** 747–769 (2002).
20. Kondo, S. & Asai, R. A reaction-diffusion wave on the skin of the marine angelfish *Pomacanthus*. *Nature* **376,** 765–768 (1995).
21. Meinhardt, H. & Gierer, A. Applications of a theory of biological pattern formation based on lateral inhibition. *J. Cell Sci.* **15,** 321–346 (1974).
22. Crampin, E. J., Gaffney, E. A. & Maini, P. K. Reaction and diffusion on growing domains: scenarios for robust pattern formation. *Bull. Math. Biol.* **61,** 1093–1120 (1999).
23. Pechmann, M., McGregor, A. P., Schwager, E. E., Feitosa, N. M. & Damen, W. G. Dynamic gene expression is required for anterior regionalization in a spider. *Proc. Natl Acad. Sci. USA* **106,** 1468–1472 (2009).
24. Patel, N. H., Condron, B. G. & Zinn, K. Pair-rule expression patterns of *even-skipped* are found in both short- and long-germ beetles. *Nature* **367,** 429–434 (1994).
25. Kanayama, M., Akiyama-Oda, Y. & Oda, H. Early embryonic development in the spider *Achaearanea tepidariorum*: Microinjection verifies that cellularization is complete before the blastoderm stage. *Arthropod Struct. Dev.* **39,** 436–445 (2010).
26. Oda, H. *et al.* Progressive activation of Delta-Notch signaling from around the blastopore is required to set up a functional caudal lobe in the spider *Achaearanea tepidariorum*. *Development* **134,** 2195–2205 (2007).
27. Akiyama-Oda, Y. & Oda, H. Cell migration that orients the dorsoventral axis is coordinated with anteroposterior patterning mediated by Hedgehog signaling in the early spider embryo. *Development* **137,** 1263–1273 (2010).
28. Akiyama-Oda, Y. & Oda, H. Early patterning of the spider embryo: a cluster of mesenchymal cells at the cumulus produces Dpp signals received by germ disc epithelial cells. *Development* **130,** 1735–1747 (2003).
29. Yamazaki, K., Akiyama-Oda, Y. & Oda, H. Expression patterns of a *twist*-related gene in embryos of the spider *Achaearanea tepidariorum* reveal divergent aspects of mesoderm development in the fly and spider. *Zoolog. Sci.* **22,** 177–185 (2005).
30. Hughes, C. L. & Kaufman, T. C. Hox genes and the evolution of the arthropod body plan. *Evol. Dev.* **4,** 459–499 (2002).
31. Akiyama-Oda, Y. & Oda, H. Axis specification in the spider embryo: *dpp* is required for radial-to-axial symmetry transformation and *sog* for ventral patterning. *Development* **133,** 2347–2357 (2006).
32. Aza-Blanc, P., Ramírez-Weber, F. A., Laget, M. P., Schwartz, C. & Kornberg, T. B. Proteolysis that is inhibited by hedgehog targets Cubitus interruptus protein to the nucleus and converts it to a repressor. *Cell* **89,** 1043–1053 (1997).
33. Benedyk, M. J., Mullen, J. R. & DiNardo, S. *odd-paired*: a zinc finger pair-rule protein required for the *timely* activation of *engrailed* and *wingless* in *Drosophila* embryos. *Genes Dev.* **8,** 105–117 (1994).
34. Irvine, K. D. & Wieschaus, E. Cell intercalation during *Drosophila* germband extension and its regulation by pair-rule segmentation genes. *Development* **120,** 827–841 (1994).
35. Gierer, A. & Meinhardt, H. A theory of biological pattern formation. *Kybernetik* **12,** 30–39 (1972).
36. Koyabu, Y., Nakata, K., Mizugishi, K., Aruga, J. & Mikoshiba, K. Physical and functional interactions between Zic and Gli proteins. *J. Biol. Chem.* **276,** 6889–6892 (2001).
37. Brewster, R., Lee, J. & Ruiz i Altaba, A. Gli/Zic factors pattern the neural plate by defining domains of cell differentiation. *Nature* **393,** 579–583 (1998).
38. Aruga, J. *et al. Zic1* regulates the patterning of vertebral arches in cooperation with *Gli3*. *Mech. Dev.* **89,** 141–150 (1999).
39. Cumberledge, S. & Krasnow, M. A. Intercellular signalling in *Drosophila* segment formation reconstructed *in vitro*. *Nature* **363,** 549–552 (1993).
40. Ingham, P. W. Localized hedgehog activity controls spatial limits of *wingless* transcription in the *Drosophila* embryo. *Nature* **366,** 560–562 (1993).
41. Ntini, E. & Wimmer, E. A. Unique establishment of procephalic head segments is supported by the identification of cis-regulatory elements driving segment-specific segment polarity gene expression in *Drosophila*. *Dev. Genes Evol.* **221,** 1–16 (2011).
42. Peel, A. The evolution of arthropod segmentation mechanisms. *Bioessays* **26,** 1108–1116 (2004).
43. Farzana, L. & Brown, S. J. Hedgehog signaling pathway function conserved in *Tribolium* segmentation. *Dev. Genes Evol.* **218,** 181–192 (2008).
44. Chipman, A. D., Arthur, W. & Akam, M. Early development and segment formation in the centipede, *Strigamia maritima* (Geophilomorpha). *Evol. Dev.* **6,** 78–89 (2004).
45. Patel, N. H., Kornberg, T. B. & Goodman, C. S. Expression of *engrailed* during segmentation in grasshopper and crayfish. *Development* **107,** 201–212 (1989).
46. Tabata, T., Eaton, S. & Kornberg, T. B. The *Drosophila hedgehog* gene is expressed specifically in posterior compartment cells and is a target of *engrailed* regulation. *Genes Dev.* **6,** 2635–2645 (1992).
47. Baker, N. E. Localization of transcripts from the *wingless* gene in whole Drosophila embryos. *Development* **103,** 289–298 (1988).
48. Rhinn, M. & Brand, M. The midbrain—hindbrain boundary organizer. *Curr. Opin. Neurobiol.* **11,** 34–42 (2001).
49. Rouillard, J. M., Zuker, M. & Gulari, E. OligoArray 2.0: design of oligonucleotide probes for DNA microarrays using a thermodynamic approach. *Nucleic Acids Res.* **31,** 3057–3062 (2003).
50. Tamura, K., Dudley, J., Nei, M. & Kumar, S. MEGA4: Molecular Evolutionary Genetics Analysis (MEGA) software version 4.0. *Mol. Biol. Evol.* **24,** 1596–1599 (2007).
51. Aruga, J. *et al.* A wide-range phylogenetic analysis of Zic proteins: implications for correlations between protein structure conservation and body plan complexity. *Genomics* **87,** 783–792 (2006).
52. Niimi, T., Kuwayama, H. & Yaginuma, T. Larval RNAi applied to the analysis of postembryonic development in the ladybird beetle, *Harmonia axyridis*. *J. Insect Biotechnol. Sericology* **74,** 95–102 (2005).

Acknowledgements

We thank F. Matsuzaki for plasmid DNA, K. Fujimoto and H. Matsuura for helpful discussions and comments on the manuscript, and A. Noda for technical assistance. This work was supported in part by KAKENHI 20570217 (H.O.) and a JSPS Research Fellowship (Y.A.).

Author contributions

M.K., Y.A. and H.O. designed and performed most of the experiments. O.N., H.T. and K.A. performed a part of the EST analyses. M.K., Y.A. and H.O. discussed the data and wrote the manuscript.

Additional information

Accession codes: The *A. tepidariorum* EST data have been deposited in the DNA Data Bank of Japan under accession numbers FY216297 to FY225483 and FY368221 to FY381845. The microarray data have been deposited in the Gene Expression Omnibus database under accession number GSE26468. Nucleotide sequences for the *A. tepidariorum* genes are available from the DNA Data Bank of Japan under the following accession numbers: *At-opa*, AB605264; *At-ci*, AB605263; *At-six3-1*, AB605265.

Supplementary Information accompanies this paper at http://www.nature.com/naturecommunications

Competing financial interests: The authors declare no competing financial interests.

Reprints and permission information is available online at http://npg.nature.com/reprintsandpermissions/

How to cite this article: Kanayama, M. *et al.* Travelling and splitting of a wave of hedgehog expression involved in spider-head segmentation. *Nat. Commun.* 2:500 doi: 10.1038/ncomms1510 (2011).